International Journal of Nanomedicine

Dovepress
open access to scientific and medical research

Open Access Full Text Article

ORIGINAL RESEARCH

Montmorillonite-norfloxacin nanocomposite intended for healing of infected wounds

This article was published in the following Dove Press journal:
International Journal of Nanomedicine

Fatima García-Villén[1]
Angela Faccendini[2]
Carola Aguzzi[1]
Pilar Cerezo[1]
Maria Cristina Bonferoni[2]
Silvia Rossi[2]
Pietro Grisoli[2]
Marco Ruggeri[2]
Franca Ferrari[2]
Giuseppina Sandri[2]
Cesar Viseras[1]

[1]Department of Pharmacy and Pharmaceutical Technology, Faculty of Pharmacy, University of Granada, Campus of Cartuja, Granada, Spain; [2]Department of Drug Sciences, Faculty of Pharmacy, University of Pavia, Pavia 27100, Italy

Background: Chronic cutaneous wounds represent a major issue in medical care and are often prone to infections.

Purpose: The aim of this study was the design of a clay mineral-drug nanocomposite based on montmorillonite and norfloxacin (NF, antimicrobial drug) as a powder for cutaneous application, to enhance wound healing in infected skin lesions.

Methods: The nanocomposite has been prepared by means of an intercalation solution procedure. Adsorption isotherm, solid-state characterization of the nanocomposite, drug loading capacity and its release have been performed. Moreover, cytocompatibility, in vitro fibroblast proliferation and antimicrobial activity against *Pseudomonas aeruginosa* and *Staphylococcus aureus* were assessed.

Results: The clay drug adsorption isotherm demonstrates that the mechanism of NF intercalation into montmorillonite galleries is the adsorption as one single process, due to the charge–charge interaction between protonated NF and negatively charged montmorillonite edges in the interlayer space. Nanocomposite is biocompatible and it is characterized by antimicrobial activity greater than the free drug: this is due to its nanostructure and controlled drug release properties.

Conclusion: Considering the results obtained, NF–montmorillonite nanocomposite seems a promising tool to treat infected skin lesions or skin wounds prone to infection, as chronic ulcers (diabetic foot, venous leg ulcers) and burns.

Keywords: montmorillonite, norfloxacin, nanocomposite, solid state characterization, wound healing

Introduction

Wound repair is a complex and tightly regulated physiological process: different cell types, including immune cells, are involved. Wound healing includes homeostasis stage (clotting and immune activation), inflammation (recruitment of neutrophilis and macrophages, production of cytokine and growth factor), proliferation phase, tissue neoformation (reepithelialization, angiogenensis and granulation) and subsequent remodeling of neoformed-tissue.[1] Considering the crucial barrier role of the skin, nonhealing wounds (such as venous leg ulcers, diabetic foot ulcers, arterial insufficiency and pressure ulcers) and burns impose substantial morbidity and mortality, deeply affecting the quality of life with high economic burden[2]

Severe cutaneous wounds represent a major issue in medical care, with approximately 300 million chronic and 100 million traumatic wound patients worldwide. Moreover, chronic wounds affect roughly 37 million of patients globally. Only in the USA in 2017,[3] the skin wounds led to an estimated direct health care cost of

Correspondence: Giuseppina Sandri
Department of Drug Sciences, University of Pavia, Viale Taramelli 12, Pavia 27100, Italy
Tel +39 038 298 7728
Email giuseppina.sandri@unipv.it

Cesar Viseras
Department of Pharmacy and Pharmaceutical Technology, Faculty of Pharmacy, University of Granada, Campus of Cartuja, 18071 s/n, Granada, Spain
Tel +3 495 824 9551
Email cviseras@ugr.es

submit your manuscript | www.dovepress.com
DovePress
http://doi.org/10.2147/IJN.S208713

$ 75 billion and an indirect cost of $ 11 billion. The population aging is likely to dramatically increase the incidence of chronic wounds due to the rising prevalence of type 2 diabetes, peripheral vascular disease and metabolic syndrome. In addition, surgery, more common in the elder population, could cause risk of wound complication especially in patients affected by diabetes.

While acute wounds generally heal without significant interventions, chronic wounds are challenging and are characterized by an intrinsic inability to heal.

The presence of microbial contamination occurring at wound bed significantly and deeply alter the normal recovery phases, leading to a possible impairment of the healing path and finally to nonhealing wounds. Moreover, among skin wounds, burns require special attention because they are often prone to infections and to abnormal scarring.[1]

The employment of antimicrobial agents, particularly antibiotics, in the treatment of nonhealing wounds is particularly controversial due to the possible rising of resistance. However, the nanoparticle-based approach, creating antimicrobial nanotherapeutics, seems a valid option to eliminate bacterial infections, avoiding antimicrobial resistance. In fact, it is reported that nanomaterials interact with bacteria and microorganisms upon multiple interactions such as electrostatic attraction, hydrophobic and Van der Waals forces through surface interactions. Moreover, the physicochemical properties of nanomaterials allow multiple pathways to interact with microorganisms, and this makes them promising candidates to achieve enhanced therapeutic efficacy against multidrug-resistant infections[4] In literature, different therapeutic approaches based on nanostructures and several types of nanomaterials (including electrospun nanofibers, hydrogel, showed improved antibacterial properties) are reported.[5–9] These systems are generally polymer-based and prepared with high energy and sophisticated processes.

Recently, the studies focused on nanocomposites based on clay minerals and drugs and/or biopolymers evidence the capability of these to interact with biological structures and open opportunities for tissue engineering and in particular for wound healing. Nanocomposites are prepared with simple procedures (spontaneous absorption of organic moieties into/onto clay following the mixture of the components in solution) easy to scale up. Moreover, the various characteristics of clay minerals in terms of the composition may offer a range of possibilities to develop systems able to facilitate both antimicrobial activity of loaded antibacterial drugs, mainly due to the capability to decrease water activity[10–12] and cell adhesion, proliferation and neotissue formation.[13,14]

Given this premise, the aim of this study is to design and develop nanocomposite based on montmorillonite (VHS, clay mineral) and norfloxacin (NF, antimicrobial drug) as a powder for cutaneous application intended for the treatment of infected wounds to enhance their healing.

NF is a synthetic antibacterial fluoroquinolone, active against a broad spectrum of Gram-positive and Gram-negative aerobic bacteria. Its mechanism of action consists in the inhibition of DNA gyrase enzyme causing an interruption of deoxyribonucleic acid synthesis.[15] In the literature, it is proposed as a prophylactic drug in wound healing, sometimes as a component of scaffolds and wound dressings.[15–18]

A NF-montmorillonite nanocomposite was prepared by means of intercalation technique in order to obtain a powder characterized by means of adsorption isotherm and solid-state, drug loading capacity and release and antimicrobial properties.[16–22]

Materials and methods

Materials

NF (Sigma Aldrich-Merck, Italy) and a pharmaceutical grade montmorillonite (VHS) (Veegum® HS, Vanderbilt, USA) were used. VHS was dried in oven (approximately 40°C) for at least 48 hrs prior to be used.

Methods

Clay-drug adsorption isotherm

The intercalation solution technique has been chosen as the methodology to study the adsorption of NF onto VHS. Firstly, a fixed amount of clay mineral (100 mg) were dispersed into 5 mL of a glacial acetic acid:water (1:1) to achieve the dissolution of NF (initial concentrations of drug (C_0) ranging from $5 \cdot 10^{-5}$ to $1 \cdot 10^{-2}$ M). These dispersions were protected from light, stirred (150 rpm) in a thermostatic bath (25°C ±1°C) for 24 hrs and subsequently centrifuged (9000 rpm, 45 mins) in order to separate the solid phase containing the nanocomposite (VHS-NF). At this point, the equilibrium concentration of NF in the supernatant (C_e) was determined at 273 nm by UV spectroscopy (UV-Vis spectrophotometer Lambda 25, Perkin Elmer, Italy). It was assumed that the difference between C_0 and C_e corresponded to the amount of NF adsorbed onto VHS and the amount of drug retained per gram of clay was calculated. The obtained results were mathematically fitted (TableCurve 2D, Systat Software Inc., UK) to obtain the

monolayer adsorption capacity of the clay and the adsorption rate constant, according to a mechanist model able to describe the adsorption of drug molecules onto solid inorganic surfaces.[13–25]

Solid state characterization

X-ray powder diffraction (XRPD) analysis was carried out using a diffractometer (X'Pert Pro model, Malven Panalytical) equipped with a solid-state detector (X'Celerator) and a spinning sample holder. The diffractogram patterns were recorded using random oriented mounts with CuKα radiation, operating at 45 kV and 40 mA, in the range 4–60 º2θ.

Fourier-transform infrared spectroscopy (FT-IR) spectra of the powdery samples were obtained with a JASCO 6,200 apparatus equipped with a Ge ATR. All analyses were performed from 400 to 4,000 cm^{-1} with a resolution of 2 cm^{-1}, and results processed with Spectra Manager v2 software.

Thermogravimetric analysis (TGA) (mod. TGA-50H, Shimadzu) was performed using a vertical oven and a precision of 0.001 mg. Approximately 40 mg of each sample were weighted in aluminum sample pans. The experiments were performed in 30–950°C range, atmospheric air and a heating rate of 10°C/min. Additionally, differential scanning calorimetry (DSC) analyses were done in a Mettler Toledo and using aluminum crucibles. The temperature range was defined between 30ºC and 400ºC at a heating rate of 10ºC/min. All the analyses were done in atmospheric air.

Measurements of zeta potential (ζ) of both the clay and the nanocomposite were performed in an aqueous solution with a concentration 0.05% w/V by using a Zetasizer Nano ZS90 apparatus (Malvern Panalytical, USA).

High-Resolution Transmission Electron Microscopy was performed by means of a FEI Titan G2 60–300 ultra-high-resolution transmission electron microscope coupled with analytical electron microscopy (AEM) performed with a SUPER-X silicon-drift windowless energy-dispersive X-ray spectroscopy detector. AEM spectra were saved in mode scanning transmission electron microscopy with a high-angle annular dark field detector. X-ray chemical element maps were also collected. The samples were directly deposited onto copper grids (300 mesh coated by farmvar/carbon film, Agar Scientific).

Drug release

NF released from nanocomposite and NF-free drug dissolution were assessed by means of HPLC-UV/DAD (PerkinElmer Series 200) apparatus using as stationary phase Zorbax Esclipse XDB-C8 column (4.6 mm × 150 mm, silica particle size 5 μm) at 25°C, as mobile phase 7:15:78 (% v/v) acetonitrile/methanol/citric acid (0.4 M), fluxed at 1 mL/min (time of analysis 15 mins). The quantification was assessed at 275 nm, as maximum absorption wavelength.[21] The method was linear in the range of 200–1 μg/mL with R^2 higher than 0.995.

An exact amount of nanocomposite or free drug was dispersed in 3 mL of saline solution (NaCl 0.9% w/v). At prefixed times, 500 μL of dissolution medium was collected and the total volume replaced. Each sample was filtered (HA 0.22 μm, Millipore) before HPLC analysis.

Antibacterial activity measurements

The antimicrobial activity of nanocomposite compared to NF as a free drug was evaluated against the bacteria strains *Staphylococcus aureus* ATCC 6538 and *Pseudomonas aeruginosa* ATCC 15442. In particular, killing time was determined as the exposure time required to kill a standardized microbial inoculum.[26] Bacteria used for killing time evaluation were grown overnight in Tryptone Soya Broth (Oxoid; Basingstoke) at 37°C. The bacteria cultures were centrifuged at 2,000 rpm for 20 mins to separate cells from broth and then suspended in PBS (pH 7.3). The suspension was diluted to adjust the number of cells to 1×10^7–1×10^8 CFU/ml.

An exact amount of nanocomposite VHS-NF or NF was added to the microorganism suspensions to obtain 5 μg/mL NF concentrations.

For each microorganism, a suspension was prepared in PBS without drug and used as control. Bacterial suspensions were incubated at 37°C. Viable microbial counts were evaluated after contact for 0, 5 and 24 hrs with the samples and microorganism suspensions grown in the same conditions and used as control.

The bacterial colonies were enumerated in Tryptone Soya Agar (Oxoid; Basingstoke) after incubation at 37°C for 24 hrs.

The microbiocidal effect value was calculated for each test organisms and contact times according to the following equation[27]

$$ME = \log N_c - \log N_d$$

where N_c is the number of CFU of the control microbial suspension and N_d is the number of CFU of the microbial suspension in presence of drug.

In vitro biocompatibility: fibroblasts

Biocompatibility (cytotoxicity) was evaluated using fibroblasts (normal human dermal fibroblasts, from juvenile foreskin from 2 to 5 passages, PromoCell, WVR, Italy).

Fibroblasts were grown in DMEM (Lonza, I), 10% v/v (FBS (EuroClone, Italy) and penicillin/streptomycin solution (pen/strep, 100 UI/100 µm/mL, Sigma Aldrich-Merck, Italy)

VHS (1.2 mg/mL), NF (0.1 mg/mL) and VHS-NF (VHS: 1.2 mg/mL and NF 0.1 mg/mL) were suspended/solubilized in cell culture medium and put in contact with the cells in suspension just after cell seeding in 96-well plate at seeding density of 35,000 cells/well. Fibroblasts were grown for 2 days. Fibroblast growth on tissue culture plastic was considered as standard growth (control).

At prefixed end point, cell growth was assessed by means of MTT test. Briefly, the medium was removed and 50 µL of MTT solution (Sigma Aldrich, Italy) at 2.5 mg/mL concentration in Hank's Buffered Salt Solution pH 7.4 was added to cover each scaffold for 3 hrs. Subsequently, MTT solution was removed from each well, and the substrates were washed with 200 µL of PBS. After the removal of PBS, 100 µL of DMSO was put in each well, and the absorbance was assayed at 570 nm by means of an ELISA plate reader (Imark Absorbance Reader, Biorad, Italy), with a reference wavelength of 690 nm. Cell viability was expressed as optical density (OD).

Statistical analysis

Statistical differences were evaluated by means of Mann-Whitney (Wilcoxon) W test (Statgraphics Centurion XV, Statistical Graphics Corporation, MD, USA). Differences were considered significant at $p<0.05$, and each significant p-value is reported in the captions.

Results and discussion

Clay-drug adsorption isotherm

Equilibrium adsorption isotherm is shown in Figure 1, where experimental points are plotted as n^s (moles of NF retained per gram of VHS) vs C_e (mol/l). The kinetic model used to fit the adsorption data is expressed by Equation (1) (Table 1), which describes drug adsorption as one single process. Montmorillonite is a phyllosilicate based on two tetrahedral sheets of silica sandwiching a central octahedral sheet of alumina spaced out interlayer spaces (galleries). On this basis, protonated NF molecules interact to the active sites of VHS located at edges and within interlayer space of montmorillonite, thus forming a drug monolayer onto the clay mineral interlayer surface.[28] Figure 1 shows that the obtained theoretical curve satisfactorily described the experimental points, as confirmed by the calculated correlation coefficient ($R^2>0.99$, Table 1). Additionally, the relatively high value of kinetic equilibrium constant (k) (Table 1) can be ascribed to great stability of the resultant VHS-NF system.

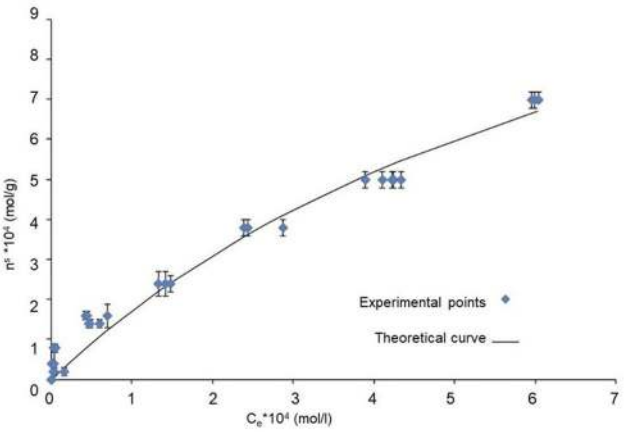

Figure 1 Equilibrium adsorption isotherm of NF and VHS (mean values ± s.d.; n=3).
Abbreviations: NF, norfloxacin; VHS, montmorillonite.

Table 1 Fitting equation and parameters for the adsorption of NF onto VHS

Equation (1)*	R^2	n^s_m	k
$n^s = \frac{k^s_m}{k+1}$	0.9959	0.0007±0.00002	130.4±0.43

Notes: *N^s: mol of NF per gram of VHS (mol/g); n^s_m: monolayer retention capacity (mol/g); C: equilibrium concentration (mol/l); k: kinetic equilibrium constant (mean values ± s.d.; n=3).
Abbreviations: NF: norfloxacin; VHS: montmorillonite.

Solid-state characterizations

X-ray diffractogram patterns of the nanohybrid and pristine components are plotted in Figure 2. VHS diffractogram shows reflections ascribable to a highly pure homoionic Na montmorillonite, as previously described.[16,24,29,30]

In particular, VHS shows d001 basal reflection at 7.5º 2θ which indicates an interlayer space of 12 Å according to Bragg's law. These results are consistent with the literature.[24,31] Diffractogram of VHS-NF also shows typical reflections of montmorillonite with the exception of the basal reflection d001, which shifts to lower 2θ values (5,94º 2θ) in comparison with the pristine clay mineral. The corresponding interlayer space is expanded (≅15 Å), indicating the presence of NF molecules adsorbed into clay mineral structure. Moreover, this new basal reflection turns to be sharper and more intense in comparison with VHS basal reflection,

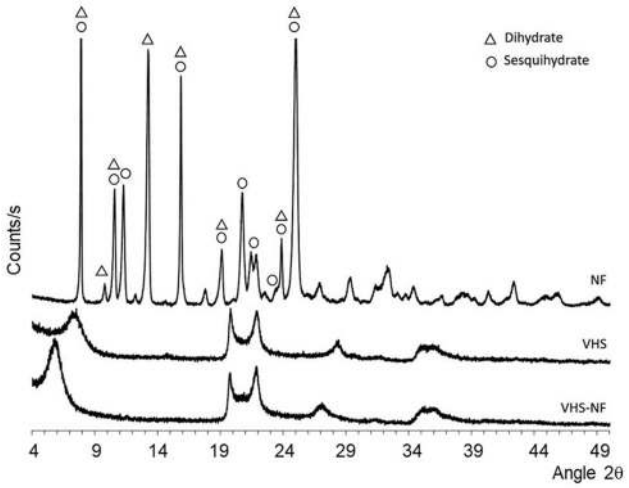

Figure 2 XRPD diffraction patterns of NF, VHS and VHS-NF.
Abbreviations: NF, norfloxacin; VHS, montmorillonite; VHS-NF, montmorillonite/norfloxacin nanocomposite.

which is an indicator of a highly ordered VHS-NF nanohybrid structure. Diffractogram of NF has been found to be a combination of both anhydrous and sesquihydrate forms (Figure 2).[32–34] Nonetheless, any of these reflections are observed in VHS-NF diffraction pattern, indicating the absence of crystalline drug on the nanohybrid surface. The XRPD analysis suggests that the nanocomposite is characterized by NF intercalation into the VHS galleries.

Figure 3 reports the FTIR spectra of VHS-NF in comparison to NF and VHS. The infrared spectrum of NF shows typical bands of a hydrated form of NF. In particular, the broad bands between 3,600 and 3,250 cm^{-1} belong to hydration water stretching (O-H stretching vibration, at about 3404 cm^{-1}) together with N-H vibrations of the

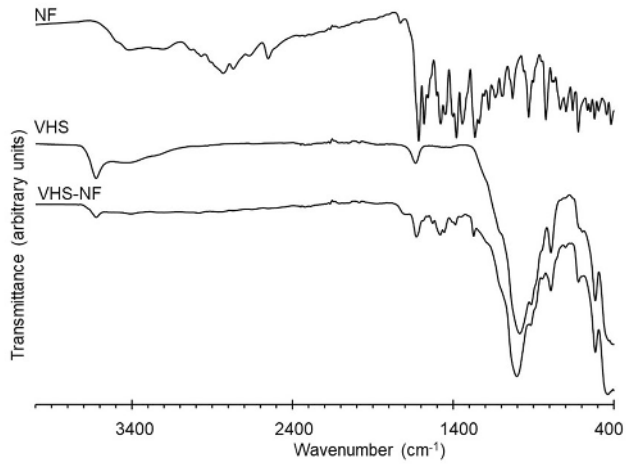

Figure 3 FT-IR spectra of NF, VHS and VHS-NF.
Abbreviations: NF, norfloxacin; VHS, montmorillonite; VHS-NF: montmorillonite/norfloxacin nanocomposite.

piperazine ring. The vibration of methyl group, methylene of ethyl side chain and piperazine groups determine multiple and more defined bands in 3,070–2,500 cm^{-1}. A shoulder at 2,500 cm^{-1} is attributable to hydrogen bonded O–H groups, and this also confirms the hydrate state of NF. Band detected at 1,728 cm^{-1} belongs to the C=O stretch of the carboxylic acid.[32,35,36] The first and intense band in the fingerprint region belongs to NF quinolone ring vibration located between 1,600 and 1,650 cm^{-1}.[32] The vibrations of C=C of the aromatic ring are also located in this area (1,400–1,600 cm^{-1}). Moreover, the band at 1,030 cm^{-1} is attributable to C-F vibration.[35] Regarding VHS, vibrational band at 3,622 cm^{-1} belongs to octahedral layer-OH groups (Al-OH-Al, Al-OH-Mg and Mg-OH-Mg vibrations) typical of clay minerals. Moreover, the broad band around 3,400 cm^{-1} are due to the stretching of OH from hydration H_2O molecules located in the interlayer space of VHS. Moreover, H_2O molecules coordinated to the VHS exchangeable cations create a band al 1,632 cm^{-1}. The most intense band of the VHS spectrum, located at 985 cm^{-1}, is due to Si-O-Si in-plane vibration for layered silicates. Out-of-plane Si-O-Si stretching is responsible for the shoulder appearing at 1,100 cm^{-1}. On the other hand, the overlapped band at 914 cm^{-1} is related to Si-O-Al stretching mode, while bending vibration of Si-O-Al occurs at 512 cm^{-1}.[24,29,30,37]

Vibrational bands of the octahedral Al-OH-Al, Al-OH-Mg and Mg-OH-Mg are also present in the VHS-NF. The adsorption of NF in the VHS interlayer space produces a displacement of the hydrated exchangeable cations, thus reducing the intensity of the H_2O band around 3,400 cm^{-1}.[35] Moreover, the presence of the drug in the nanohybrid can be identified by its typical vibrational bands located between 1,760 and 1,200 cm^{-1}, all of them coinciding with the NF spectrum. Particularly, the band at 1,702 cm^{-1} belongs to C=O of the carboxylic acid of NF. From 1,200 cm^{-1} onwards, the intense vibrations of the clay mineral obscure the NF bands in the same region. Nonetheless, the bands in 3,070–2,500 cm^{-1} range, which correspond to N-H and CH_2 of the drug, are not visible in the VHS-NF spectrum. This disappearance can be related to the stiffening of the corresponding functional group due to the position of adsorbed NF molecules in the interlayer space of VHS.

The TGA analysis of NF showed total drug decomposition before 630°C (Figure 4 – high panel). The first weight loss gradually occurs in the temperature range from 30°C to 196°C, with an inflection point at 100°C. This step is due to

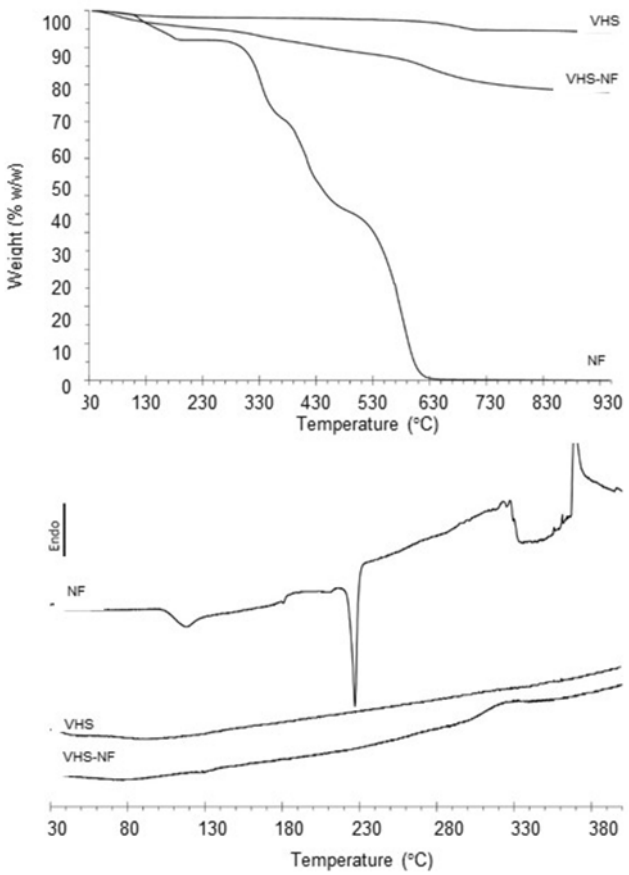

Figure 4 Thermal analysis (TGA – high panel curves and DSC – low panel curves) of NF, VHS and VHS-NF samples.
Abbreviations: NF, norfloxacin; VHS, montmorillonite; VHS-NF, montmorillonite/norfloxacin nanocomposite.

the evaporation of water and corresponds to the first endothermic event of the corresponding DSC curve (Figure 4 – low panel). Nonetheless, the presence of an inflection point could be related to different types of crystallization water. In fact, different hydrated forms of NF have been reported in literature, such as dihydrate and sesquihydrate, among others.[38] In particular, water evaporation of NF dihydrate form is described as a two different step process although this is not visible in DSC profile and on the contrary it is evident in TGA profile.[38] These results are related to the presence of both dihydrate and sesquihydrate forms (as confirmed by XRPD diffraction peaks) having overlapped steps of H_2O molecule evaporation in DSC. The sharp and intense endothermic peak located at 227°C (T onset 218°C) corresponds to NF melting point, confirmed by the absence of weight loss in the TGA curve of NF. Decomposition of the drug starts at 300°C according to TGA profile and three overlapped steps (inflection point at ~370°C and ~500°C) are attributable to the loss of different functional groups of the NF molecule ($6C_2H_2$+3NO+HF+1/2H_2)[38] and/or gaseous products.[39] Parallelly DSC thermogram (low panel) shows an exothermic event at 370 °C, and this is in coincidence of the first inflection point of the TGA corresponding to NF decomposition.

TGA thermogram of VHS (Figure 4 – high panel) shows a first slight weight loss of 2% (w/w), which corresponds to a small amount of hydration water. Moreover, a typical clay mineral dehydroxylation step[40] is present with an onset at about 600°C and an offset at 720°C, accounting 3% (w/w) weight loss. From 800°C onwards, there is no signal that could be related to VHS impurity decomposition (such as quartz, mullite, corderite, cristobalite),[40] to confirm its high purity. DSC thermogram of VHS confirms its stability in the temperature range evaluated (Figure 4 – low panel).

VHS-NF nanocomposite shows TGA thermogram characterized by overlapped events (Figure 4 – high panel). In particular, it is evident that water loss is followed by the decomposition of NF and dehydroxylation of clay. Considering that NF fully decomposes before 630ºC, the difference in weight loss between VHS and VHS-NF reveals that VHS-NF is characterized by 16% (w/w) NF loading. Moreover, NF is present in an amorphous state in VHS-NF since melting event is not evident in VHS-NF DSC thermogram (Figure 4 – low panel) while the actual NF loading can be justified by the exothermic phenomenon observable at 300–345°C.

A 0.05% w/v VHS aqueous suspension is characterized by zeta potential of −43.5±0.9 mV, thus confirming the negative net charge of the clay. A 0.05% w/v VHS-NF nanocomposite aqueous suspension shows a zeta potential of −15.9±0.3 mV. VHS and NF probably interact via electrostatic bonds partially shielding the negative charges located into VHS galleries. The dissolution of NF in acetic acid during the nanocomposite preparation causes the protonation of its nitrogen atom in the piperazine ring. In this condition, NF in solution, positively charged, can interact with the negatively charges in the interlayer space of VHS, normally compensated by exchangeable cations increasing the zeta potential. Similar results were reported for clay–cationic moieties interaction products.[39,40]

High-resolution TEM microphotographs of VHS sample (Figure 5A) show the typical layered morphology of montmorillonite. The EDX analysis performed in the marked zone (red square) confirms the nature of VHS, thanks to the presence of Si, Al and O, together with Mg and Fe and the typical exchangeable cations (Na, K and Ca).

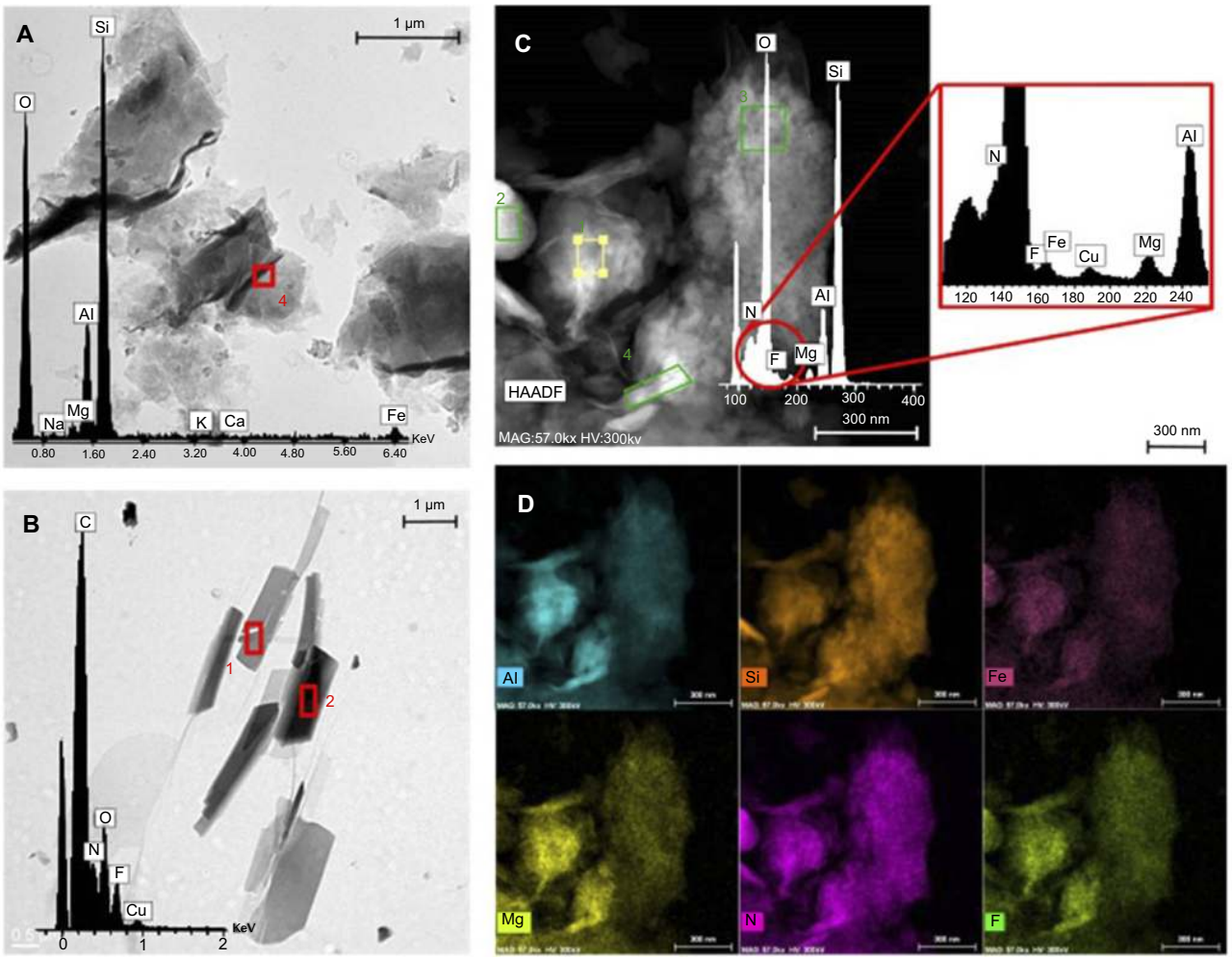

Figure 5 TEM microphotographs and EDX analysis of VHS (**A**), NF (**B**) and VHS-NF (**C**) together with EDX mapping of VHS-NF (**D**).
Abbreviations: NF, norfloxacin; VHS, montmorillonite; VHS-NF, montmorillonite/norfloxacin nanocomposite.

NF (Figure 5B) microphotographs confirm NF crystallinity and agree with XRDP results. Moreover, the EDX analysis evidences the presence of C, O and N (typical of organic compounds) and that of F peculiar of NF molecule.

VHS-NF nanocomposite (Figure 5C) shows a morphology similar to that of VHS. The NF crystals are not detectable in this sample, in agreement with XRPD results (no peak of NF diffraction in VHS-NF sample, Figure 2) although the NF presence in nanocomposite is confirmed by means of the EDX analysis. The elemental composition evidences the characteristic components of montmorillonite (Si, Al, Mg) and those of organic compounds (C, N, O); moreover, F is also detectable as NF indicator. Additionally, EDX maps (Figure 5D) corroborate not only the presence of VHS and NF in nanocomposite but also the homogeneous distribution of NF into montmorillonite, confirming the presence of NF monolayer adsorbed onto the interlayer spaces, as resulted from adsorption studies.

Drug release

Figure 6 reports the NF release profiles (%) evaluated for NF and VHS-NF nanocomposite. The dissolution of NF from free drug is very rapid and reaches 80% within the first hour and the plateau value in 2 hrs at 100% of NF release.

VHS-NF shows a significantly lower NF release profile and the whole dose is released in 48 hrs evidencing a controlled release. Considering the application (skin lesions), the capability of the system to control drug release should decrease the number of applications over time. This is an important aspect to allow the healing of lesion since the frequent medical treatment could impair the granulation tissue and new tissue formation. Moreover, the slower release profile of NF could allow to control microbial growth over time.

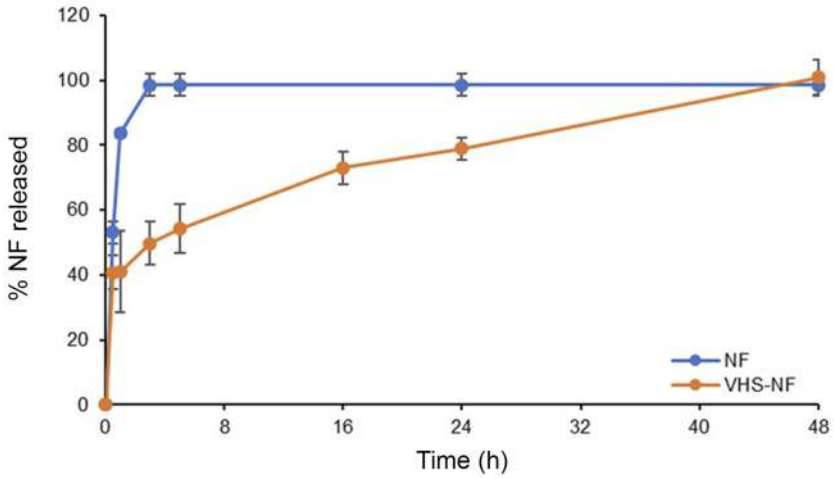

Figure 6 % of norfloxacin (NF) released from NF and VHS-NF (mean values ± s.d.; n=3).
Abbreviations: NF, norfloxacin; VHS-NF, montmorillonite/norfloxacin nanocomposite.

Antimicrobial properties

Figure 7 reports microbiocidal effect vs time profiles of NF released from NF and VHS-NF against a) *Pseudomonas aeruginosa* and b) *Staphylococcus aureus*.

Pseudomonas aeruginosa is a common Gram-negative, rod-shaped bacterium, facultative anaerobe, of considerable medical importance. It is recognized as a multidrug-resistant pathogen for its ubiquity, its intrinsically advanced antibiotic resistance mechanisms and its association with hospital-acquired infections such as various sepsis syndromes. *P. aeruginosa* is considered opportunistic insofar as serious infection often occurs during existing diseases or conditions, most notably traumatic burns.

Staphylococcus aureus is a Gram-positive, round-shaped bacterium and, as *P. aeruginosa*, it is a facultative anaerobe. It is an usual member of the microbiota of the body, frequently found on the skin, usually acting as a commensal. However, it can also become an opportunistic pathogen, being a common cause of skin infections. The onset of *S. aureus* strains antibiotic-resistant (such as methicillin-resistant *S. aureus*) is a worldwide emergence in clinical medicine.

NF is reported in the literature as effective against both *P. aeruginosa* and *S. aureus* having a MIC of 2 μg/mL in both cases.[39] However, the microbicidal effect is slightly higher against *P. aeruginosa* than that against *S. aureus*. The loading of NF in montmorillonite in VHS-NF nanocomposite significantly increases NF microbicidal effect. The increase of NF potency due to the nanocomposite is probably due to high surface area to volume ratio, which increases the contact area with target organisms.[40]

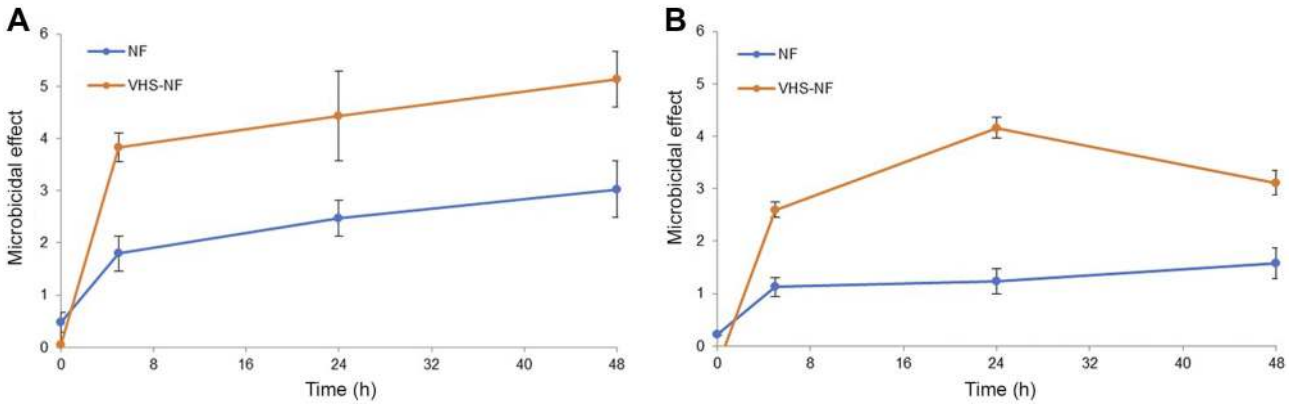

Figure 7 Microbiocidal effect vs time profiles of norfloxacin (NF) released from NF and VHS-NF against (**A**) *Pseudomonas aeruginosa* and (**B**) *Staphylococcus aureus* (mean values ± s.d.; n=3).
Abbreviations: NF, norfloxacin; VHS-NF, montmorillonite/norfloxacin nanocomposite.

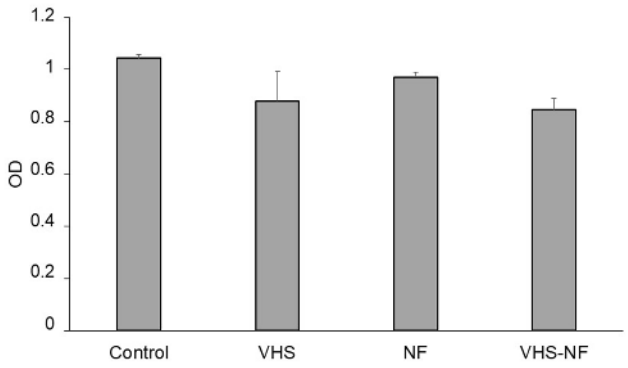

Figure 8 Bioavailability (OD) evaluated for VHS (1.2 mg/mL), NF (0.1 mg/mL) and VHS-NF (VHS: 1.2 mg/mL and NF 0.1 mg/mL) compared to the control (growth medium, standard growth conditions) (mean values ± s.d.; n=8) (Statistical analysis W test: control vs VHS-NF: p=0.030).
Abbreviations: NF, norfloxacin; VHS, montmorillonite; VHS-NF, montmorillonite/norfloxacin nanocomposite.

Fibroblast in vitro biocompatibility

Figure 8 reports bioavailability (OD, optical density) evaluated for VHS (1.2 mg/mL), NF (0.1 mg/mL) and VHS-NF (VHS: 1.2 mg/mL and NF 0.1 mg/mL). VHS and NF are characterized by OD values not significantly different from the control (growth medium, standard growth conditions). The nanocomposite, VHS-NF, is characterized by OD significantly lower than that of the control although it is higher than 80% and this is normally considered as the lower limit for the cytocompatibility.

VHS, NF and VHS-NF are characterized by no significantly different OD to suggest similar behaviour. Anyhow, it should be considered that the cytocompatibility is assayed to a 20-fold concentration higher than that considered for antimicrobial assay. This evidences that nanocomposite does not impair fibroblast growth also at concentrations higher than those effective against *P. aeruginosa* and *S. aureus* as assessed in the antimicrobial assay.

Conclusions

NF is loaded into montmorillonite to have a nanocomposite by means of adsorption mechanism, as one single process. In particular, protonated NF molecules interact with the active sites of montmorillonite located at edges and within its interlayer space, thus forming a drug monolayer onto the clay mineral interlayer surface. NF in the nanocomposites is in an amorphous state, and its loading is homogeneous and causes an expansion of montmorillonite interlayer spaces. Moreover, the nanocomposite causes a prolonged NF release over time. The nanocomposite is characterized by good biocompatibility in vitro toward fibroblasts, and it is able to increase antimicrobial potency of the free drug against *P. aeruginosa* and *S. aureus*, Gram-negative and Gram-positive bacteria, respectively, that are often a concurrent cause of wound chronicization, leading to a possible impairment of the healing path and finally to nonhealing wounds.

NF-montmorillonite nanocomposite demonstrates to possess suitable properties as a tool to enhance wound healing in infected wounds: the possibility to use a flexible dosage, as a powder for cutaneous application, should also allow easy administration, depending on lesion dimensions.

Disclosure

The authors report no conflicts of interest in this work.

References

1. Mafazzal Jahromi MA, Sahandi Zangabad P, Moosavi Basri SM, et al. Nanomedicine and advanced technologies for burns: preventing infection and facilitating wound healing. *Adv Drug Deliv Rev*. 2018;123:33–64. doi:10.1021/acsami.9b01508
2. Stejskalova A, Almquist BD. Using biomaterials to rewire the process of wound repair. *Biomater Sci*. 2017;5:1421–1434. doi:10.1002/ppsc.201800420
3. Lim HW, Collins SA, Resneck JS, et al. The burden of skin disease in the United States. *J Am Acad Dermatol*. 2017;76:958–972, e952. doi:10.1039/C8TB02491J
4. Gupta A, Mumtaz S, Li C-H, et al. Combatting antibiotic-resistant bacteria using nanomaterials. *Chem Rev Soc*. 2019;48:415–427. doi:10.1021/acsami.8b09656
5. Lv D, Wang R, Tang G, et al. Ecofriendly electrospun membranes loaded with visible-light-responding nanoparticles for multifunctional usages: highly efficient air filtration, dye scavenging, and bactericidal activity. *ACS Appl Mater Interfaces*. 2019;11:12880–12889. doi:10.1007/s10570-017-1409-4
6. Sun L, Li A, Hu Y. et al. Self-assembled fluorescent and antibacterial GHK-Cu nanoparticles for wound healing applications part. *Part Syst Charact*;2019. 1800420. doi:10.1002/ppsc.201800420
7. Gao S, Tang G, Hua D, et al. Stimuli-responsive bio-based polymeric systems and their applications. *J Mater Chem B*. 2019;7:709–729. doi:10.1039/C8TB02491J
8. Ding Q, Xu X, Yue Y, et al. Nanocellulose-mediated electroconductive self-healing hydrogels with high strength, plasticity, viscoelasticity, stretchability, and biocompatibility toward multifunctional applications. *ACS Appl Mater Interfaces*. 2018;10:27987–28002. doi:10.1021/acsami.8b09656
9. Han J, Yue Y, Wu Q, et al. Effects of nanocellulose on the structure and properties of poly(vinyl alcohol)-borax hybrid foams. *Cellulose*. 2017;24:4433–4448. doi:10.1007/s10570-017-1409-4
10. Bramhill J, Ross S, Ross G. Bioactive nanocomposites for tissue repair and regeneration: a review. *Int J Environ Res Public Health*. 2017;14:1–21. doi:10.3390/ijerph14010066
11. Sandri G, Bonferoni MC, Ferrari F, et al. Montmorillonite-chitosan-silver sulfadiazine nanocomposites for topical treatment of chronic skin lesions: in vitro biocompatibility, antibacterial efficacy and gap closure cell motility properties. *Carbohydr Polym*. 2014;102:970–977. doi:10.1016/j.carbpol.2013.10.029
12. Naumenko EA, Guryanov ID, Yendluri R, Lvov YM, Fakhrullin RF. Clay nanotube-biopolymer composite scaffolds for tissue engineering. *Nanoscale*. 2016;8:7257–7271. doi:10.1039/C6NR00641H

13. Sandri G, Aguzzi C, Rossi S, et al. Halloysite and chitosan oligosaccharide nanocomposite for wound healing. *Acta Biomater*. 2017;57:216–224. doi:10.1016/j.actbio.2017.05.032
14. Sandri G, Bonferoni MC, Rossi S, et al. Clay minerals for tissue regeneration, repair, and engineering. In: *Wound Healing Biomaterials*. Ed. Agren M. Chapter 19, Vol. 2. Sawston, Cambridge, UK: Woodhead Publishing, Elsevier, 2016:385–402. Functional Biomaterials.
15. Wiles JA, Bradbury BJ, Pucci MJ. New quinolone antibiotics: a survey of the literature from 2005 to 2010. *Exp Opin Therap Patents*. 2010;20:1295–1319. doi:10.1517/13543776.2010.505922
16. Nakamura M, Nishida T, Mishima H, Otori T. Effects of antimicrobials on corneal epithelial migration. *Curr Eye Res*. 1993;12 (8):733–740. doi:10.3109/02713689308995769
17. Malipeddi VR, Dua K, Sara UVS, et al. Comparative evaluation of transdermal formulations of norfloxacin with silver sulfadiazine cream, USP, for burn wound healing property. *J Burns Wounds*. 2006;5:e4.
18. Mpharm KD, Ramana MV, Sara UVS, et al. Preparation and evaluation of transdermal plasters containing norfloxacin: a novel treatment for burn wound healing. *Eplasty*. 2010;10:e44.
19. Tian Z, Zhang Y, Liu X, Chen C, Guiltinan MJ, Allcock HR. Biodegradable polyphosphazenes containing antibiotics: synthesis, characterization, and hydrolytic release behavior. *Polym Chem*. 2013;4:1826. doi:10.1039/c2py21064a
20. Galperin A, Smith K, Geisler NS, Bryers JD, Ratner BD. Precision-porous polyHEMA-based scaffold as an antibiotic-releasing insert for a scleral bandage. *ACS Biomater Sci Eng*. 2015;1:593–600. doi:10.1021/acsbiomaterials.5b00133
21. Mahmoud AA. Salama AH Norfloxacin-loaded collagen/chitosan scaffolds for skin reconstruction: preparation, evaluation and in-vivo wound healing assessment. *Eur J Pharm Sci*. 2016;83:155–165. doi:10.1016/j.ejps.2015.12.026
22. Rusanu A, Tamaş AI, Vulpe R, Rusu A, Butnaru M, Vereştiuc L. Biocompatible and biodegradable hydrogels based on chitosan and gelatin with potential applications as wound dressings. *J Nanosci Nanotechnol*. 2017;17:4584–4591. doi:10.1166/jnn.2017.14298
23. Carazo E, Borrego-Sánchez A, García-Villén F, et al. Assessment of halloysite nanotubes as vehicles of isoniazid. *Colloids Surf B Biointerfaces*. 2017;160:337–344. doi:10.1016/j.colsurfb.2017.09.036
24. Carazo E, Borrego-Sánchez A, García-Villén F, et al. Adsorption and characterisation of palygorskite-isoniazid nanohybrids. *Appl Clay Sci*. 2018;160:180–185. doi:10.1016/j.clay.2017.12.027
25. Viseras C, Aguzzi C, Cerezo P, Bedmar MC. Biopolymer–clay nanocomposites for controlled drug delivery. *Mat Sci Technol*. 2008;24:1020–1026. doi:10.1179/174328408X341708
26. Samanidou VF, Demetriou CE, Papadoyannis IN. Direct determination of four fluoroquinolones, enoxacin, norfloxacin, ofloxacin, and ciprofloxacin, in pharmaceuticals and blood serum by HPLC. *Anal Bioanal Chem*. 2003;375(5):623–629. doi:10.1007/s00216-003-1749-9
27. Rossi S, Marciello M, Sandri G, et al. Wound dressings based on chitosans and hyaluronic acid for the release of chlorhexidine diacetate in skin ulcer therapy. *Pharm Dev Technol*. 2007;12:415–422. doi:10.1080/10837450701366903
28. Viseras MT, Aguzzi C, Cerezo P, Viseras C, Valenzuela C. Equilibrium and kinetics of 5-aminosalicylic acid adsorption by halloysite. *Micropor Mesopor Mat*. 2008;108:112–116. doi:10.1016/j.micromeso.2007.03.033
29. Borrego-Sánchez A, Carazo E, Aguzzi C, Viseras C, Sainz-Díaz CI. Biopharmaceutical improvement of praziquantel by interaction with montmorillonite and sepiolite. *Appl Clay Sci*. 2018;160:173–179. doi:10.1016/j.clay.2017.12.024
30. Aguzzi C, Sandri G, Bonferoni C, et al. Solid state characterisation of silver sulfadiazine loaded on montmorillonite/chitosan nanocomposite for wound healing. *Colloids Surf B Biointerfaces*. 2014;113:152–157. doi:10.1016/j.colsurfb.2013.08.043
31. Tunç S, Duman O. Preparation and characterization of biodegradable methyl cellulose/montmorillonite nanocomposite films. *Appl Clay Sci*. 2010;48:414–424. doi:10.1016/j.clay.2010.01.016
32. Mazuel C. Norfloxacin. In: Florey K, Brittain H, Mazzo D, et al., editors. *Analytical Profiles of Drug Substances and Excipients*. 1st ed. London Academic Press Inc; 1991:557–600.
33. Katdare AV, Ryan JA, Bavitz JF, Erb DM, Guillory JK. Characterization of hydrates of Norfloxacin. *Mikrochim Acta*. 1986; III:1–12. doi:10.1007/BF01196816
34. Puigjaner C, Barbas R, Portell A, Font-Bardia M, Alcobé X, Prohens R. Revisiting the solid state of norfloxacin. *Cryst Growth Des*. 2010;10:2948–2953. doi:10.1021/cg9014898
35. Földvári M. Handbook of thermogravimetric system of minerals and its use in geological practice. In: Gyula M, Dezsö Simonyi OP, Tamás F, editors. Vol. 213. Budapest: Innova-Print Kft; 2011.
36. Barry AL, Jones RN, Thornsberry C, Ayers LW, Gerlach EH, Sommers HM. Antibacterial activities of ciprofloxacin, norfloxacin, oxolinic acid, cinoxacin, and nalidixic acid. *Antimicrob Agents Chemother*. 1984;25:633–637. doi:10.1128/aac.25.5.633
37. Baptista PV, McCusker MP, Carvalho A, et al. Nano-strategies to fight multidrug resistant bacteria—"A battle of the titans". *Front Microbiol*. 2018;9:1441. doi:10.3389/fmicb.2018.01441
38. Kumar M, Curtis A, Hoskins C. Application of nanoparticle technologies in the combat against anti-microbial resistance. *Pharmaceutics*. 2018;10:11. doi:10.3390/pharmaceutics10010011
39. Norrby SR, Jonsson M. Antibacterial activity of norfloxacin. *Antimicrob Agents Chemother*. 1983;23:15–18. doi:10.1128/AAC.23.1.15
40. Wang Y, Zhu L, Dong Z, et al. Preparation and stability study of norfloxacin-loaded solid lipid nanoparticle suspensions. *Colloids Surf B Biointerfaces*. 2012;98:105–111. doi:10.1016/j.colsurfb.2012.05.006